

Multimapping Image-to-Image Translation via Learning Disentanglement

Xiaoming Yu^{1,2}, Yuanqi Chen^{1,2}, Thomas Li^{1,3}, Shan Liu⁴, and Ge Li^{✉1,2}

¹School of Electronics and Computer Engineering, Peking University ²Peng Cheng Laboratory

³Advanced Institute of Information Technology, Peking University ⁴Tencent America

xiaominguo@pku.edu.cn, cyq373@pku.edu.cn

tli@aiit.org.cn, shanl@tencent.com, geli@ece.pku.edu.cn

Abstract

Recent advances of image-to-image translation focus on learning the one-to-many mapping from two aspects: multi-modal translation and multi-domain translation. However, the existing methods only consider one of the two perspectives, which makes them unable to solve each other's problem. To address this issue, we propose a novel unified model, which bridges these two objectives. First, we disentangle the input images into the latent representations by an encoder-decoder architecture with a conditional adversarial training in the feature space. Then, we encourage the generator to learn multi-mappings by a random cross-domain translation. As a result, we can manipulate different parts of the latent representations to perform multi-modal and multi-domain translations simultaneously. Experiments demonstrate that our method outperforms state-of-the-art methods. Code will be available at <https://github.com/Xiaoming-Yu/DMIT>.

1 Introduction

Image-to-image (I2I) translation is a broad concept that aims to translate images from one domain to another. Many computer vision and image processing problems can be handled in this framework, e.g. image colorization [16], image inpainting [41], style transfer [47], etc. Previous works [16, 47, 42, 18, 25] present the impressive results on the task with deterministic one-to-one mapping, but suffer from mode collapse when the outputs correspond to multiple possibilities. For example, in the season transfer task, as shown in Fig. 1, a summer image may correspond to multiple winter scenes with different styles of lighting, sky, and snow. To tackle this problem and generalize the applicable scenarios of I2I, recent studies focus on one-to-many translation and explore the problem from two perspectives: multi-domain translation [21, 3, 26], and multi-modal translation [48, 23, 15, 44, 41].

The multi-domain translation aims to learn mappings between each domain and other domains. Under a single unified framework, recent works realize the translation among multiple domains. However, between the two domains, what these methods have learned are still deterministic one-to-one mappings, thus they fail to capture the multi-modal nature of the image distribution within the image domain. Another line of works is the multi-modal translation. BicycleGAN [48] achieves the one-to-many mapping between the source domain and the target domain by combining the objective of cVAE-GAN [22] and cLR-GAN [2, 5, 7]. MUNIT [15] and DRIT [23] extend the method to learn two one-to-many mappings between the two image domains in an unsupervised setting, i.e., domain A to domain B and vice versa. While capable of generating diverse and realistic translation outputs, these methods are limited when there are multiple image domains to be translated. In order to adapt to the new task, the domain-specific encoder-decoder architecture in these methods needs to be duplicated to the number of image domains. Moreover, they assume that there is no correlation of the styles between domains, while we argue that they could be aligned as shown in Fig. 1. Besides,

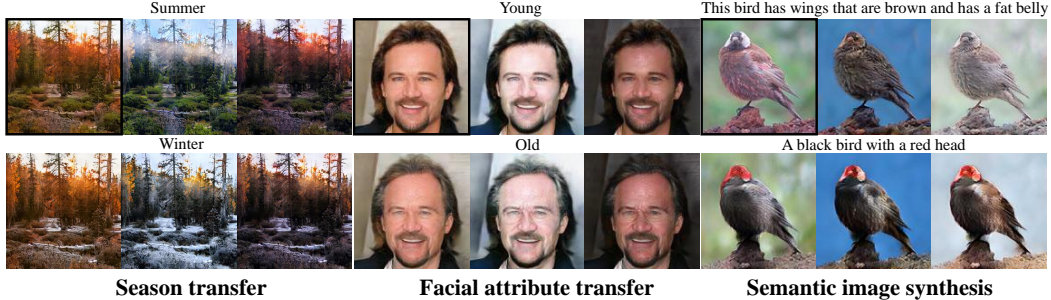


Figure 1: **Multi-mapping image-to-image translation.** The images with a black border are the input images, and other images are generated by our method. The images on the same column have the same style, which indicates that the styles between image domains could be aligned.

existing one-to-many mapping methods usually assume the state of the domain is finite and discrete, which limits their application scenarios.

In this paper, we focus on bridging the objectives of multi-domain translation and multi-modal translation with an unsupervised unified framework. For clarity, we refer our task to as **multi-mapping translation**. Simultaneous modeling for these two problems not only makes the framework more efficient but also encourages the model to learn efficient representations for diverse translations.

To instantiate the idea, as shown in Fig. 2(d), we assume that the images can be disentangled into **two latent representation spaces**: a content space \mathcal{C} and a style space \mathcal{S} , and propose an encoder-decoder architecture to learn the disentangled representations. Our assumption is developed by the shared latent space assumption [25], but we disentangle the latent space into two separate parts to model the multi-modal distribution and to achieve cross-domain translation. Unlike partially-shared latent space assumption [15, 23], that treats style information as domain-specific, the styles between image domains are aligned in our assumption, as shown in Fig. 1. Specifically, the style representations in this work are low-dimensional vectors which do not contain spatial information and hence can only control the global appearance of the outputs. By using a unified style encoder to learn style representations and thus fully utilizing samples of all image domains, the sample space of our style representation is denser than that learned from only one specific image domain. As for content representations, they are feature maps capturing the spatial structure information across domains. To mitigate the effects of distribution shift among domains, we eliminate domain-specific information in content representations via conditional adversarial learning. To achieve multi-mapping translation using a single unified decoder, we concatenate the disentangled style representations with the target domain label, then adopt the style-based injection method to render the content representations to our desired outputs. Through learning the inverse mapping of disentanglement, we can change the domain label to translate an image to the specific domain or modify the style representation to produce multi-modal outputs. Furthermore, we can extend our framework to a more challenging task of **semantic image synthesis** whose domains can be considered as an uncountable set and cannot be modeled by existing I2I approaches.

The contributions of this work are summarized as follows:

- We introduce an unsupervised unified multi-mapping framework, which unites the objectives of multi-domain and multi-modal translations.
- By aligning latent representations among image domains, our model is efficient in learning disentanglement and performing finer image translation.
- Experimental results show our model is superior to the state-of-the-art methods.

2 Related Work

Image-to-image translation. The problem of I2I is first defined by Isola *et al.* [16]. Based on the generative adversarial networks [11, 29], they propose a general-purpose framework (pix2pix) to handle I2I. To get rid of the constraint of paired data in pix2pix, [47, 42, 18] utilize the cycle-

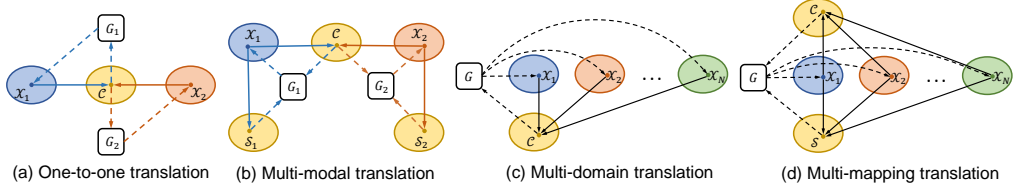


Figure 2: **Comparisons of unsupervised I2I translation methods.** Denote \mathcal{X}_k as the k -th image domain. The solid lines and dashed lines represent the flow of encoder and generator respectively. The lines with the same color indicate they belong to the same module.

Table 1: Comparisons with recent works on unsupervised image-to-image translation

	Multi-modal translation	Multi-domain translation	Multi-mapping translation	Unified structure	Feature disentanglement	Representation alignment
UNIT	-	-	-	-	-	✓
StarGAN	-	✓	-	✓	-	-
MUNIT	✓	-	-	-	✓	Partial
DRIT	✓	-	-	-	✓	Partial
SingleGAN	✓	✓	-	-	-	-
Ours	✓	✓	✓	✓	✓	✓

consistency for the stability of training. UNIT [25] assumes a shared latent space for two image domains. It achieves unsupervised translation by learning the bijection between latent and image spaces using two generators. However, these methods only learn the one-to-one mapping between two domains and thus produce deterministic output for an input image. Recent studies focus on multi-domain translation [21, 3, 44, 26] and multi-modal translation [48, 41, 23, 15, 41, 44, 33]. Unfortunately, neither multi-modal translation nor multi-domain translation considers the other’s scenario, which makes them unable to solve the problem of each other. Table 1 shows a feature-by-feature comparison among various unsupervised I2I models. Different from the aforementioned methods, we explore a combination of these two problems rather than separation, which makes our model more efficient and general purpose. Concurrent with our work, several independent researches [4, 35, 39] also tackle the multi-mapping problem from different perspectives.

Representation disentanglement. To achieve a finer manipulation in image generation, disentangling the factors of data variation has attracted a great amount of attention [20, 13, 2]. Some previous works [21, 26] aim to learn domain-invariant representations from data across multiple domains, then generate different realistic versions of an input image by varying the domain labels. Others [23, 15, 10] focus on disentangling the images into domain-invariant and domain-specific representations to facilitate learning diverse cross-domain mappings. Inspired by these works, we attempt to disentangle the images into solely independent parts: content and style. Moreover, we align these representations among image domains, which allows us to utilize rich content and style from different domains and manipulate the translation in finer detail.

Semantic image synthesis. The goal of semantic image synthesis is to generate an image to match the given text while retaining the irrelevant information from the input image. Dong *et al.* [6] train a conditional GAN to synthesize a manipulated version of the image given an original image and a target text description. To preserve text-irrelevant contents of the original image, Paired-D GAN [28] proposes to model the foreground and background distribution with different discriminators. TAGAN [32] introduces a text-adaptive discriminator to pay attention to the regions that correspond to the given text. In this work, we treat the image set with the same text description as an image domain. Thus the domains are countless and each domain contains very few images in the training set. Benefit from the unified framework and the representation alignment among different domains, we can tackle this problem in our unified multi-mapping framework.

3 Proposed Method

Let $\mathcal{X} = \bigcup_{k=1}^N \mathcal{X}_k \subset \mathbb{R}^{H \times W \times 3}$ be an image set that contains all possible images of N different domains. We assume that the images can be disentangled to two latent representations $(\mathcal{C}, \mathcal{S})$. \mathcal{C} is

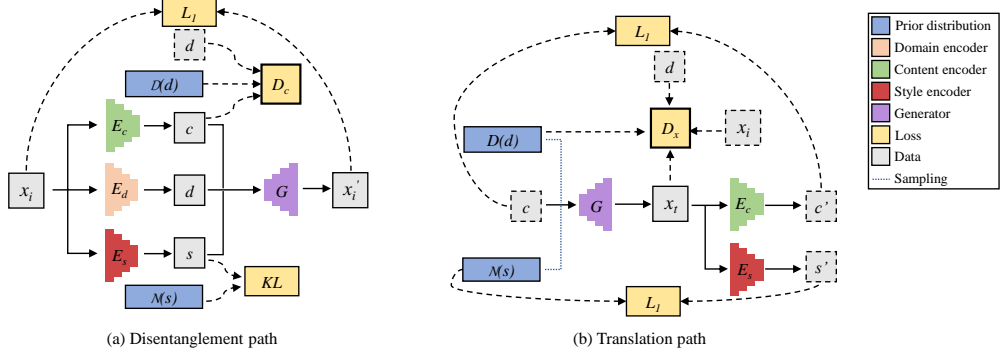


Figure 3: **Overview.** (a) The disentanglement path learns the bijective mapping between the disentangled representations and the input image. (b) The translation path encourages to generate diverse outputs with possible styles in different domains.

the set of contents excluded from the variation among domains and styles, and \mathcal{S} is the set of styles that is the rendering of the contents. Our goal is to train a unified model that learns multi-mappings among multiple domains and styles. To achieve this goal, we also define \mathcal{D} as a set of domain labels and treat \mathcal{D} as another disentangled representations of the images. Then we propose to learn mapping functions between images and disentangled representations $\mathcal{X} = (\mathcal{C}, \mathcal{S}, \mathcal{D})$.

As illustrated in Fig. 3(a), we introduce the content encoder $E_c : \mathcal{X} \rightarrow \mathcal{C}$ that maps an input image to its content, and the encoder style $E_s : \mathcal{X} \rightarrow \mathcal{S}$ that extracts the style of the input image. To unify the formulation, We also denote the determined mapping function between \mathcal{X} and \mathcal{D} as the domain label encoder $E_d : \mathcal{X} \rightarrow \mathcal{D}$ which is organized as a dictionary¹ and extracts the domain label from the input image. The inversely disentangled mapping is formulated as the generator $G : (\mathcal{C}, \mathcal{S}, \mathcal{D}) \rightarrow \mathcal{X}$. As a result, with any desired style $s \in \mathcal{S}$ and domain label $d \in \mathcal{D}$, we can translate an input image $x_i \in \mathcal{X}$ to the corresponding target $x_t \in \mathcal{X}$

$$x_t = G(E_c(x_i), s, d). \quad (1)$$

3.1 Network Architecture

Encoder. The content encoder E_c is a fully convolutional network that encode the input image to the spatial feature map c . Since the small output stride used in E_c , c retains rich spatial structure information of input image. The style encoder E_s consists of several residual blocks followed by global average pooling and fully connected layers. By global average pooling, E_s removes the structure information of input and extract the statistical characteristics to represent the input style [9]. The final style representation s are constructed as a low-dimensional vector by the reparameterization trick [20].

Generator. Motivated by recent style-based methods [8, 14, 17, 15, 44], we adopt a style-based generator G to simultaneous model for multi-domain and multi-modal translations. Specifically, the generator G consists of several residual blocks followed by several deconvolutional layers. Each convolution layer in residual blocks is equipped with CBIN [44, 45] for information injection.

Discriminator. Unlike previous works [23, 15, 44] that apply different discriminators for different image domains, we propose to adopt a unified conditional discriminator for different domains. Since the large distribution shift between image domains in I2I, it is challenging to use a unified discriminator. Inspired by the style-based generator, we apply CBIN to the discriminator to extend the capacity of our model. For more details of our network, we refer the reader to our supplementary materials.

3.2 Learning Strategy

Our proposed method encourages the bijective mapping between the image and the latent representations while learning disentanglement. Fig. 3 presents an overview of our model, whose learning

¹Since encoder E_d has a deterministic mapping, it is no need for joint training with E_d in our training stage.

process can be separated into disentanglement path and translation path. The disentanglement path can be considered as an encoder-decoder architecture that uses conditional adversarial training on the latent space. Here we enforce the encoders to encode the image into the disentangled representations, which can be mapped back to the input image by the conditional generator. The translation path enforces the generator to capture the full distribution of possible outputs by a random cross-domain translation.

Disentanglement path. To disentangle the latent representations from image x_i , we adopt cVAE [36] as the base structure. To align the style representations across visual domains and constrain the information of the styles [1], we encourage the distribution of styles of all domains to be as close as possible to a prior distribution.

$$\mathcal{L}_{cVAE} = \lambda_{KL} \mathbb{E}_{x_i \sim \mathcal{X}} [KL(E_s(x_i) || q(s))] + \lambda_{rec} \mathbb{E}_{x_i \sim \mathcal{X}} [\|G(E_c(x_i), E_s(x_i), E_d(x_i)) - x_i\|_1]. \quad (2)$$

To enable stochastic sampling at test time, we choose the prior distribution $q(s)$ to be a standard Gaussian distribution $\mathcal{N}(0, I)$. As for the content representations, we propose to perform conditional adversarial training in the content space to address the distribution shift issue of the contents among domains. This process encourages E_c to exclude the information of the domain d in content c

$$\mathcal{L}_{GAN}^c = \mathbb{E}_{x_i \sim \mathcal{X}} [\log(D_c(E_c(x_i), E_d(x_i))) + \mathbb{E}_{d \sim (\mathcal{D} - \{E_d(x_i)\})} [\log(1 - D_c(E_c(x_i), d))]]. \quad (3)$$

the overall loss of the disentanglement path is

$$\mathcal{L}_{D-Path} = \mathcal{L}_{cVAE} + \mathcal{L}_{GAN}^c. \quad (4)$$

Translation path. The disentanglement path encourages the model to learn the content c and the style s with a prior distribution. But it leaves two issues to be solved: First, limited by the number of training data and the optimization of KL loss, the generator G may sample only a subset of \mathcal{S} and generate the images with specific domain labels in the training stage [37]. It may lead to poor generations when sampling s in the prior distribution \mathcal{N} and d that does not match the test image, as discussed in [48]. Second, the above training process lacks efficient incentives for the use of styles, which would result in low diversity of the generated images. To overcome these issues and encourage our generator to capture a complete distribution of outputs, we first propose to randomly sample domain labels and styles in the prior distributions, in order to cover the whole sampling space at training time. Then we introduce the latent regression [2, 48] to force the generator to utilize the style vector. The regression can also be applied to the content c to separate the style s from c . Thus the latent regression can be written as

$$\mathcal{L}_{reg} = \mathbb{E}_{\substack{c \sim c \\ s \sim \mathcal{N} \\ d \sim \mathcal{D}}} [\|E_s(G(c, s, d)) - s\|_1] + \mathbb{E}_{\substack{c \sim c \\ s \sim \mathcal{N} \\ d \sim \mathcal{D}}} [\|E_c(G(c, s, d)) - c\|_1]. \quad (5)$$

To match the distribution of generated images to the real data with sampling domain labels and styles, we employ conditional adversarial training in the pixel space

$$\begin{aligned} \mathcal{L}_{GAN}^x = & \mathbb{E}_{x_i \sim \mathcal{X}} [\log(D_x(x_i, E_d(x_i))) + \mathbb{E}_{d \sim (\mathcal{D} - \{E_d(x_i)\})} [\frac{1}{2} \log(1 - D_x(x_i, d))] \\ & + \mathbb{E}_{s \sim \mathcal{N}} [\frac{1}{2} \log(1 - D_x(G(E_c(x_i), s, d), d))]]. \end{aligned} \quad (6)$$

Note that we also discriminate the pair of real image x_i and mismatched target domain label d , in order to encourage the generator to generate images that correspond to the given domain label. The final objective of the translation is

$$\mathcal{L}_{T-Path} = \lambda_{reg} \mathcal{L}_{reg} + \mathcal{L}_{GAN}^x. \quad (7)$$

By combining both training paths, the full objective function of our model is

$$\min_{G, E_c, E_s} \max_{D_c, D_x} \mathcal{L}_{D-Path} + \mathcal{L}_{T-Path}. \quad (8)$$

4 Experiments

We compare our approach against recent one-to-many mapping models in two tasks, including season transfer and semantic image synthesis. For brevity, we refer to our method, Disentanglement for Multi-mapping Image-to-Image Translation, as DMIT. In the supplementary material, we provide additional visual results and extend our model to facial attribute transfer [24] and sketch-to-photo [43].



Figure 4: Qualitative comparison of season transfer. The first column shows the input image. Each of the remaining columns shows four outputs with the specified season from a method. Each image pair for the specified season reflects the diversity within the domain.

4.1 Datasets

Yosemite summer ↔ winter. The unpaired dataset is provided by Zhu *et al.* [47] for evaluating unsupervised I2I methods. We use the default image size 256×256 and training set in all experiments. The domain label(summer/winter) is organized as a one-hot vector.

CUB. The Caltech-UCSD Birds (CUB) [38] dataset contains 200 bird species with 11,788 images that each have 10 text captions [34]. We preprocess the CUB dataset according to the method in [40]. The captions are encoded as the domain labels by the pretrained text encoder proposed in [40].

4.2 Season Transfer

Season transfer is a coarse-grained translation task that aims to learn the mapping between summer and winter. We compare our method against five baselines, including:

- Multi-domain models: StarGAN [3] and StarGAN* that adds the noise vector into the generator to encourage the diverse outputs.
- Multi-modal models: MUNIT [15], DRIT [23], and *version-c* of SingleGAN [44].

In the above models, MUNIT, DRIT and SingleGAN require a pair of GANs for summer → winter and winter → summer severally. StarGAN-based models and DMIT only use a unified structure to learn the bijection mapping between two domains. To better evaluate the performance of multi-domain and multi-modal mappings, we propose to test inter-domain and intra-domain translations separately.

As the qualitative comparison in Fig. 4 shows, the synthesis of StarGAN has significant artifacts and suffer from mode collapse caused by the assumption of deterministic cross-domain mapping. With the noise disturbance, the quality of generated images by StarGAN* has improved, but the results are still lacking in diversity. All of the multi-modal models produce diverse results. However, without utilizing the style information between different domains, the generated images are monotonous and only differ in simple modes, such as global illumination. We observe that MUNIT is hard to converge and to produce realistic season transfer results due to the limited training data. DRIT and SingleGAN produce realistic results, but the images are not vivid enough. In contrast, our DMIT can use only one unified model to produce realistic images with diverse details for different image domains.

To quantify the performance, we first translate each test image to 10 targets by sampling styles from prior distribution. Then we adopt Fréchet Inception Distance (FID) [12] to evaluate the quality of generated images, and LPIPS (official version 0.1) [46] to measure the diversity [15, 23, 48] of samples generated by same input image within a specific domain. The quantitative results shown in Table 2 further confirm our observations above. It is remarkable that our method achieves the best FID score while greatly surpassing the multi-domain and multi-modal models in LPIPS distance.

Table 2: Quantitative comparison of season transfer.

	summer → winter		summer → summer		winter → summer		winter → winter	
	FID	LPIPS	FID	LPIPS	FID	LPIPS	FID	LPIPS
StarGAN	218.78	-	233.61	-	248.29	-	224.37	-
StarGAN*	152.11	0.012	135.25	0.011	153.79	0.013	149.04	0.011
MUNIT	84.43	0.166	58.96	0.133	73.82	0.134	68.92	0.141
DRIT	58.70	0.205	49.58	0.166	53.79	0.192	57.11	0.179
SingleGAN	63.77	0.184	51.64	0.186	54.24	0.188	57.30	0.178
DMIT w/o T-Path	75.90	0.109	57.24	0.118	72.75	0.124	65.15	0.116
DMIT w/o D-Path	116.71	0.545	85.97	0.513	95.63	0.517	124.96	0.544
DMIT w/o \mathcal{L}_{GAN}^c	60.81	0.268	43.54	0.260	50.33	0.270	58.09	0.256
DMIT w/ VanillaD	63.34	0.259	44.73	0.239	50.79	0.255	60.10	0.242
DMIT w/ ProjectionD	66.50	0.289	46.92	0.301	52.4	0.293	65.66	0.299
DMIT	58.46	0.302	43.04	0.275	48.02	0.292	55.23	0.279

Ablation study. To analyze the importance of different components in our model, we perform an ablation study with five variants of DMIT.

As for the training paths, we observe that both T-Path and D-Path are indispensable. Without T-Path, the model is difficult to perform cross-domain translation as we analyzed in Section 3. In contrast, without D-Path, the generated images are blurry and unrealistic and produce meaningless diversity by the artifacts. Combining these two paths result in a trade-off of quality and diversity of images.

As for the training incentive, we observe \mathcal{L}_{GAN}^c is influential for the diversity score. Without this incentive, the visual styles are similar in summer and winter. It suggests that D_c encourages the model to eliminate the domain bias and to learn well-disentangled representations.

As for the architecture of discriminator, we evaluate two other conditional models with different information injection strategies, including vanilla conditional discriminator (VanillaD) [16, 29] that concatenates input image and conditional information together, and projection discriminator (ProjectionD) [30, 31] that projects the conditional information to the hidden activation of image. The qualitative results in Table 2 indicate that the capacity of VanillaD is limited. The images generated of DMIT with ProjectionD are diverse, but prone to contain artifacts, which leads to its lower FID score. Our full DMIT, equipped style-based discriminator, gets the balance between diversity and quality.

4.3 Semantic Image Synthesis

To further verify the potential of DMIT in mixed-modality (text and image) translation, we study on the task of semantic image synthesis. The existing I2I approaches usually assume the state of the domain is discrete, which causes them to not be able to handle this task. We compare our model with the state-of-the-art models of semantic image synthesis: SISGAN [6], Paired-D GAN [28], and TAGAN [32].

Fig. 5 shows our qualitative comparison with the baselines. Although SISGAN can generate diverse images that match the text, it is difficult to generate high-quality images. The structure and background of the images are retained well by Paired-D GAN, but the results do not match the text well. Furthermore, it can be observed that Paired-D GAN cannot produce diversity for conditional input with different samples. TAGAN presents images with acceptable semantic matching results, but the quality is unsatisfactory. By encoding the style from the input image, DMIT can well preserve the original background of the input image and generate high-quality images that match the text descriptions. Meanwhile, DMIT can also produce diverse results by sampling other style representation.

Besides to calculate FID to qualify the performance, we perform a human perceptual study on Amazon Mechanical Turk (AMT) to measure the semantic matching score. We randomly sample 2,500 images and mismatched texts for generating questions. For each comparison, five different workers are required to select which image looks more realistic and fits the given text. As shown in Table 3, DMIT gets the best of both image quality and semantic matching score. Since retaining the irrelevant information of the input image is important for semantic image synthesis, we also evaluate the reconstruction ability of different methods by transforming the input image with its corresponding text. The scores of PSNR and SSIM further demonstrate the capabilities of our method



Figure 5: Qualitative comparison of semantic image synthesis. In each column, the first row is the input image and the remaining rows are the outputs according to the above text description. In each pair of images generated by DMIT, the images in the first column are generated by encoding the style from the input image and the second column are generated by random style.

Table 3: Quantitative comparison of semantic image synthesis.

	FID	Human evaluation	PSNR	SSIM
SISGAN	67.24	15.3%	11.27	0.193
Paired-D GAN	27.62	25.2%	22.34	0.886
TAGAN	34.49	20.4%	19.01	0.736
DMIT	13.85	39.1%	25.49	0.934

in learning efficient representations. It suggests that the disentangled representations enable our model to manipulate the translation in finer detail.

4.4 Limitations

Although DMIT can perform multi-mapping translation, we observe that the style representations tend to model some global properties as discussed in [33]. Besides, we observe that the convergence rates of different domains are generally different. Further exploration will allow this work to be a general-purpose solution for a variety of multi-mapping translation tasks.

5 Conclusion

In this paper, we present a novel model for multi-mapping image-to-image translation with unpaired data. By learning disentangled representations, it is able to use the advances of both multi-domain and multi-modal translations in a holistic manner. The integration of these two multi-mapping problems encourages our model to learn a more complete distribution of possible outputs, improving the performance of each task. Experiments in various multi-mapping tasks show that our model is superior to the existing methods in terms of quality and diversity.

Acknowledgments

This work was supported in part by Shenzhen Municipal Science and Technology Program (No. JCYJ20170818141146428), National Engineering Laboratory for Video Technology - Shenzhen Division, and National Natural Science Foundation of China and Guangdong Province Scientific Research on Big Data (No. U1611461). In addition, we would like to thank the anonymous reviewers for their helpful and constructive comments.

References

- [1] Alexander A Alemi, Ian Fischer, Joshua V Dillon, and Kevin Murphy. Deep variational information bottleneck. In *ICLR*, 2017.
- [2] Xi Chen, Yan Duan, Rein Houthooft, John Schulman, Ilya Sutskever, and Pieter Abbeel. Infogan: Interpretable representation learning by information maximizing generative adversarial nets. In *NIPS*, 2016.
- [3] Yunjey Choi, Minje Choi, Munyoung Kim, Jung-Woo Ha, Sunghun Kim, and Jaegul Choo. Stargan: Unified generative adversarial networks for multi-domain image-to-image translation. In *CVPR*, 2018.
- [4] Yunjey Choi, Youngjung Uh, Jaejun Yoo, and Jung-Woo Ha. Stargan v2: Diverse image synthesis for multiple domains. *arXiv preprint arXiv:1912.01865*, 2019.
- [5] Jeff Donahue, Philipp Krähenbühl, and Trevor Darrell. Adversarial feature learning. In *ICLR*, 2016.
- [6] Hao Dong, Simiao Yu, Chao Wu, and Yike Guo. Semantic image synthesis via adversarial learning. In *ICCV*, 2017.
- [7] Vincent Dumoulin, Ishmael Belghazi, Ben Poole, Olivier Mastropietro, Alex Lamb, Martin Arjovsky, and Aaron Courville. Adversarially learned inference. In *ICLR*, 2016.
- [8] Vincent Dumoulin, Jonathon Shlens, and Manjunath Kudlur. A learned representation for artistic style. In *ICLR*, 2017.
- [9] Leon A Gatys, Alexander S Ecker, and Matthias Bethge. Image style transfer using convolutional neural networks. In *CVPR*, 2016.
- [10] Abel Gonzalez-Garcia, Joost van de Weijer, and Yoshua Bengio. Image-to-image translation for cross-domain disentanglement. In *NIPS*, 2018.
- [11] Ian Goodfellow, Jean Pouget-Abadie, Mehdi Mirza, Bing Xu, David Warde-Farley, Sherjil Ozair, Aaron Courville, and Yoshua Bengio. Generative adversarial nets. In *NIPS*, 2014.
- [12] Martin Heusel, Hubert Ramsauer, Thomas Unterthiner, Bernhard Nessler, and Sepp Hochreiter. Gans trained by a two time-scale update rule converge to a local nash equilibrium. In *NIPS*, 2017.
- [13] Irina Higgins, Loic Matthey, Arka Pal, Christopher Burgess, Xavier Glorot, Matthew Botvinick, Shakir Mohamed, and Alexander Lerchner. beta-vae: Learning basic visual concepts with a constrained variational framework. In *ICLR*, 2017.
- [14] Xun Huang and Serge Belongie. Arbitrary style transfer in real-time with adaptive instance normalization. In *ICCV*, 2017.
- [15] Xun Huang, Ming-Yu Liu, Serge Belongie, and Jan Kautz. Multimodal unsupervised image-to-image translation. In *ECCV*, 2018.
- [16] Phillip Isola, Jun-Yan Zhu, Tinghui Zhou, and Alexei A Efros. Image-to-image translation with conditional adversarial networks. In *CVPR*, 2017.
- [17] Tero Karras, Samuli Laine, and Timo Aila. A style-based generator architecture for generative adversarial networks. In *CVPR*, 2019.
- [18] Taeksoo Kim, Moonsu Cha, Hyunsoo Kim, Jung Kwon Lee, and Jiwon Kim. Learning to discover cross-domain relations with generative adversarial networks. In *ICML*, 2017.
- [19] D Kingma and J Ba Adam. A method for stochastic optimization. In *ICLR*, 2015.
- [20] Diederik P Kingma and Max Welling. Auto-encoding variational bayes. In *ICLR*, 2014.
- [21] Guillaume Lample, Neil Zeghidour, Nicolas Usunier, Antoine Bordes, Ludovic Denoyer, et al. Fader networks: Manipulating images by sliding attributes. In *NIPS*, 2017.

- [22] Anders Boesen Lindbo Larsen, Søren Kaae Sønderby, Hugo Larochelle, and Ole Winther. Autoencoding beyond pixels using a learned similarity metric. In *ICML*, 2016.
- [23] Hsin-Ying Lee, Hung-Yu Tseng, Jia-Bin Huang, Maneesh Kumar Singh, and Ming-Hsuan Yang. Diverse image-to-image translation via disentangled representations. In *ECCV*, 2018.
- [24] Ziwei Liu, Ping Luo, Xiaogang Wang, and Xiaoou Tang. Deep learning face attributes in the wild. In *ICCV*, 2015.
- [25] Ming-Yu Liu, Thomas Breuel, and Jan Kautz. Unsupervised image-to-image translation networks. In *NIPS*, 2017.
- [26] Alexander H Liu, Yen-Cheng Liu, Yu-Ying Yeh, and Yu-Chiang Frank Wang. A unified feature disentangler for multi-domain image translation and manipulation. In *NIPS*, 2018.
- [27] Xudong Mao, Qing Li, Haoran Xie, Raymond YK Lau, Zhen Wang, and Stephen Paul Smolley. Least squares generative adversarial networks. In *ICCV*, 2017.
- [28] Duc Minh Vo and Akihiro Sugimoto. Paired-d gan for semantic image synthesis. In *ACCV*, 2018.
- [29] Mehdi Mirza and Simon Osindero. Conditional generative adversarial nets. *arXiv preprint arXiv:1411.1784*, 2014.
- [30] Takeru Miyato and Masanori Koyama. cgans with projection discriminator. In *ICLR*, 2018.
- [31] Takeru Miyato, Toshiki Kataoka, Masanori Koyama, and Yuichi Yoshida. Spectral normalization for generative adversarial networks. In *ICLR*, 2018.
- [32] Seonghyeon Nam, Yunji Kim, and Seon Joo Kim. Text-adaptive generative adversarial networks: Manipulating images with natural language. In *NIPS*, 2018.
- [33] Ori Press, Tomer Galanti, Sagie Benaim, and Lior Wolf. Emerging disentanglement in auto-encoder based unsupervised image content transfer. In *ICLR*, 2019.
- [34] Scott Reed, Zeynep Akata, Bernt Schiele, and Honglak Lee. Learning deep representations of fine-grained visual descriptions. In *CVPR*, 2016.
- [35] Andrés Romero, Pablo Arbeláez, Luc Van Gool, and Radu Timofte. Smit: Stochastic multi-label image-to-image translation. In *ICCV Workshops*, 2019.
- [36] Kihyuk Sohn, Honglak Lee, and Xinchen Yan. Learning structured output representation using deep conditional generative models. In *NIPS*, 2015.
- [37] Yu Tian, Xi Peng, Long Zhao, Shaoting Zhang, and Dimitris N Metaxas. Cr-gan: Learning complete representations for multi-view generation. In *IJCAI*, 2018.
- [38] Catherine Wah, Steve Branson, Peter Welinder, Pietro Perona, and Serge Belongie. The caltech-ucsd birds-200-2011 dataset. 2011.
- [39] Yaxing Wang, Abel Gonzalez-Garcia, Joost van de Weijer, and Luis Herranz. Sdit: Scalable and diverse cross-domain image translation. In *ACM MM*, 2019.
- [40] Tao Xu, Pengchuan Zhang, Qiuyuan Huang, Han Zhang, Zhe Gan, Xiaolei Huang, and Xiaodong He. Attngan: Fine-grained text to image generation with attentional generative adversarial networks. In *CVPR*, 2018.
- [41] Dingdong Yang, Seunghoon Hong, Yunseok Jang, Tianchen Zhao, and Honglak Lee. Diversity-sensitive conditional generative adversarial networks. In *ICLR*, 2019.
- [42] Zili Yi, Hao Zhang, Ping Tan, and Minglun Gong. Dualgan: Unsupervised dual learning for image-to-image translation. In *ICCV*, 2017.
- [43] Aron Yu and Kristen Grauman. Fine-grained visual comparisons with local learning. In *CVPR*, 2014.

- [44] Xiaoming Yu, Xing Cai, Zhenqiang Ying, Thomas Li, and Ge Li. Singlegan: Image-to-image translation by a single-generator network using multiple generative adversarial learning. In *ACCV*, 2018.
- [45] Xiaoming Yu, Zhenqiang Ying, Thomas Li, Shan Liu, and Ge Li. Multi-mapping image-to-image translation with central biasing normalization. *arXiv preprint arXiv:1806.10050*, 2018.
- [46] Richard Zhang, Phillip Isola, Alexei A Efros, Eli Shechtman, and Oliver Wang. The unreasonable effectiveness of deep features as a perceptual metric. In *CVPR*, 2018.
- [47] Jun-Yan Zhu, Taesung Park, Phillip Isola, and Alexei A Efros. Unpaired image-to-image translation using cycle-consistent adversarial networks. In *ICCV*, 2017.
- [48] Jun-Yan Zhu, Richard Zhang, Deepak Pathak, Trevor Darrell, Alexei A Efros, Oliver Wang, and Eli Shechtman. Toward multimodal image-to-image translation. In *NIPS*, 2017.

A Implementation

A.1 Network Architecture

The architecture details are as follows, except that the domain label encoder E_d is organized as a dictionary without learnable parameters. We follow the notations used in [3]: h and w : height and width of the input image, n_s and n_d : dimensions of style s and domain label d , N : the number of output channels, K : kernel size, S : stride size, P : padding size, FC: fully connected layer, IN: instance normalization, LN: layer normalization, CBN: central biasing normalization, LReLU: Leaky ReLU with a negative slope of 0.2.

Part	Input → Output Shape	Layer Information
Down-sampling	$(h, w, 3) \rightarrow (h, w, 64)$	CONV-(N64, K7x7, S1, P3), IN, LReLU
	$(h, w, 64) \rightarrow (\frac{h}{2}, \frac{w}{2}, 128)$	CONV-(N128, K4x4, S2, P1), IN, LReLU
	$(\frac{h}{2}, \frac{w}{2}, 128) \rightarrow (\frac{h}{4}, \frac{w}{4}, 256)$	CONV-(N128, K4x4, S2, P1), IN, LReLU
Bottleneck	$(\frac{h}{4}, \frac{w}{4}, 256) \rightarrow (\frac{h}{4}, \frac{w}{4}, 256)$	ResBlock: CONV-(N256, K3x3, S1, P1), IN, LReLU
	$(\frac{h}{4}, \frac{w}{4}, 256) \rightarrow (\frac{h}{4}, \frac{w}{4}, 256)$	ResBlock: CONV-(N256, K3x3, S1, P1), IN, LReLU
	$(\frac{h}{4}, \frac{w}{4}, 256) \rightarrow (\frac{h}{4}, \frac{w}{4}, 256)$	ResBlock: CONV-(N256, K3x3, S1, P1), IN, LReLU
	$(\frac{h}{4}, \frac{w}{4}, 256) \rightarrow (\frac{h}{4}, \frac{w}{4}, 256)$	ResBlock: CONV-(N256, K3x3, S1, P1), IN, LReLU

Table 4: Architecture of content encoder E_c

Part	Input → Output Shape	Layer Information
Down-sampling	$(h, w, 3) \rightarrow (\frac{h}{2}, \frac{w}{2}, 64)$	CONV-(N64, K4x4, S2, P1)
	$(\frac{h}{2}, \frac{w}{2}, 64) \rightarrow (\frac{h}{4}, \frac{w}{4}, 128)$	ResBlock: CONV-(N256, K3x3, S1, P1), IN, LReLU, AvgPool-(K2x2, S2)
	$(\frac{h}{4}, \frac{w}{4}, 128) \rightarrow (\frac{h}{8}, \frac{w}{8}, 256)$	ResBlock: CONV-(N256, K3x3, S1, P1), IN, LReLU, AvgPool-(K2x2, S2)
	$(\frac{h}{8}, \frac{w}{8}, 256) \rightarrow (\frac{h}{16}, \frac{w}{16}, 256)$	ResBlock: CONV-(N256, K3x3, S1, P1), IN, LReLU, AvgPool-(K2x2, S2)
	$(\frac{h}{16}, \frac{w}{16}, 256) \rightarrow (256)$	LReLU, GlobalAvgPool
Output Layer(μ)	$(256) \rightarrow (n_s)$	FC-(256, n_s)
Output Layer($logvar$)	$(256) \rightarrow (n_s)$	FC-(256, n_s)

Table 5: Architecture of style encoder E_s

Part	Input → Output Shape	Layer Information
Bottleneck	$(\frac{h}{4}, \frac{w}{4}, 256) + (n_s + n_d) \rightarrow (\frac{h}{4}, \frac{w}{4}, 256)$	ResBlock: CONV-(N256, K3x3, S1, P1), CBIN, ReLu
	$(\frac{h}{4}, \frac{w}{4}, 256) + (n_s + n_d) \rightarrow (\frac{h}{4}, \frac{w}{4}, 256)$	ResBlock: CONV-(N256, K3x3, S1, P1), CBIN, ReLu
	$(\frac{h}{4}, \frac{w}{4}, 256) + (n_s + n_d) \rightarrow (\frac{h}{4}, \frac{w}{4}, 256)$	ResBlock: CONV-(N256, K3x3, S1, P1), CBIN, ReLu
	$(\frac{h}{4}, \frac{w}{4}, 256) + (n_s + n_d) \rightarrow (\frac{h}{4}, \frac{w}{4}, 256)$	ResBlock: CONV-(N256, K3x3, S1, P1), CBIN, ReLu
	$(\frac{h}{4}, \frac{w}{4}, 256) + (n_s + n_d) \rightarrow (\frac{h}{4}, \frac{w}{4}, 256)$	ResBlock: CONV-(N256, K3x3, S1, P1), CBIN, ReLu
Up-sampling	$(\frac{h}{4}, \frac{w}{4}, 256) \rightarrow (\frac{h}{2}, \frac{w}{2}, 128)$	DECONV-(N128, K4x4, S2, P1), LN, ReLu
	$(\frac{h}{2}, \frac{w}{2}, 128) \rightarrow (h, w, 64)$	DECONV-(N64, K4x4, S2, P1), LN, ReLu
	$(h, w, 64) \rightarrow (h, w, 3)$	CONV-(N3, K7x7, S1, P3), Tanh

Table 6: Architecture of generator G . The style s and the domain label d are injected by central biasing normalization.

Part	Input → Output Shape	Layer Information
	$(h, w, 3) \rightarrow (\frac{h}{2}, \frac{w}{2}, 64)$	CONV-(N64, K4x4, S2, P1)
Down-sampling	$(\frac{h}{2}, \frac{w}{2}, 64) + (n_d) \rightarrow (\frac{h}{4}, \frac{w}{4}, 128)$	ResBlock: CONV-(N256, K3x3, S1, P1), CBIN, LReLU, AvgPool-(K2x2, S2)
	$(\frac{h}{4}, \frac{w}{4}, 128) + (n_d) \rightarrow (\frac{h}{8}, \frac{w}{8}, 256)$	ResBlock: CONV-(N256, K3x3, S1, P1), CBIN, LReLU, AvgPool-(K2x2, S2)
Output Layer	$(\frac{h}{8}, \frac{w}{8}, 256) \rightarrow (\frac{h}{8}, \frac{w}{8}, 1)$	CONV-(N1, K1x1, S1, P0)

Table 7: Architecture of discriminator D_c and D_x . The domain label d are injected by central biasing normalization.

A.2 Training Details

We train all our models with Adam optimizer [19], setting the learning rate of 0.0001 and exponential decay rates $(\beta_1, \beta_2) = (0.5, 0.999)$. To keep each loss close in magnitude, the hyper-parameters are set as follows: $\lambda_{rec} = 10$, $\lambda_{reg} = 1$, $\lambda_{KL} = 0.01$. The batch size is set as one for season transfer and sketch-to-photo tasks, and eight for semantic image synthesis and facial attribute transfer. Besides, we adopt multi-scale strategy proposed by Zhu *et al.* [48] to discriminate the real and fake images in different scales. Since the distributions of content c are still changing, we use the objective of LSGAN [27] to stabilize the training of D_c . Besides, we replace the standard adversarial loss of D_x with hinge version [31] to accelerate the convergence. All of the models are trained on a single NVIDIA TITAN V GPU.

B Additional Experiment Results

B.1 Season Transfer

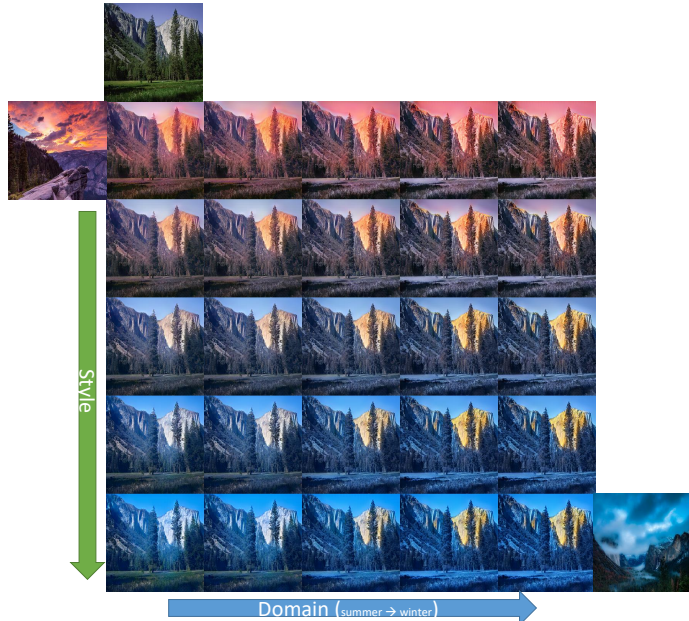


Figure 6: **The interpolation on latent representations.** In this experiment, the content representation is extracted from the image of the first row and the style representations are extracted from the first and final columns. The images on the same row have the same style representation and images on the same column have the same domain label representation.

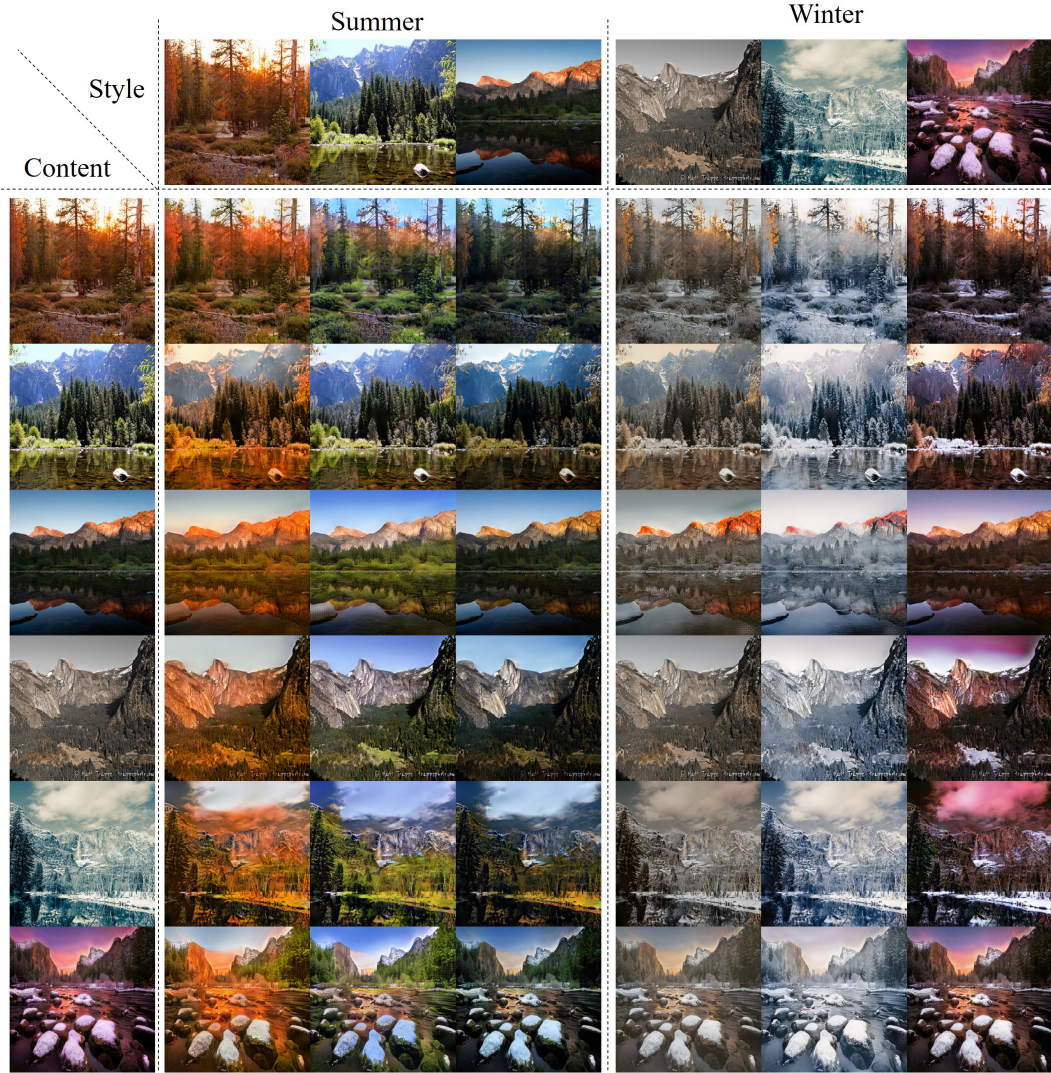


Figure 7: Example-guided image translation. In this experiment, the content representation is extracted from the image of the first column and the style representations are extracted from the first row. The images on the same row have the same content representation and images on the same column have the same style representation.

B.2 Semantic Image Synthesis

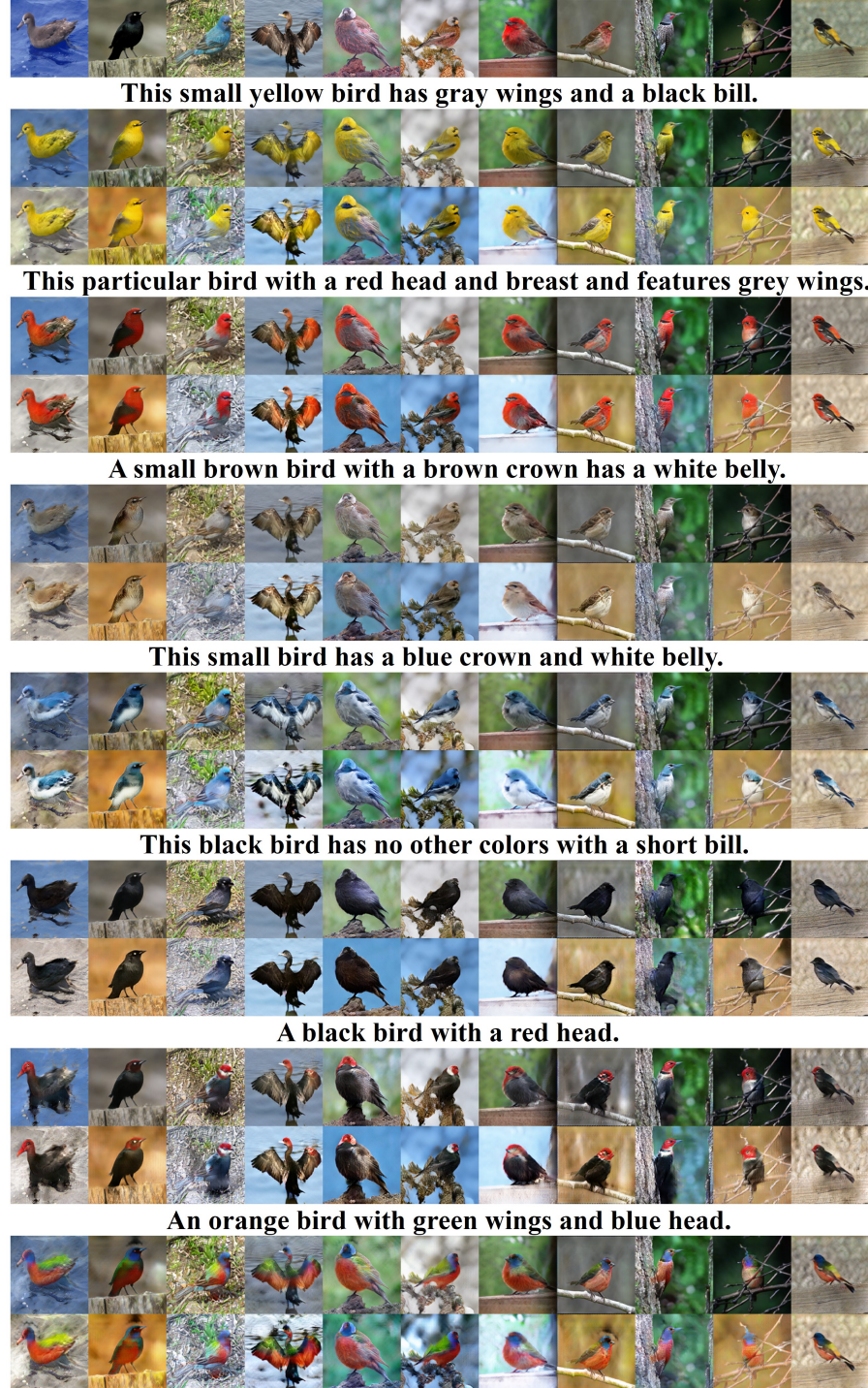


Figure 8: **Semantic image synthesis on CUB [38].** The first row shows the input images. Each of the remaining rows presents the translation results according to the text description.

B.3 Facial Attribute Transfer

we perform the facial attribute transfer on the The CelebFaces Attributes(CelebA) dataset [24]. CelebA dataset contains a large number of celebrity images. We preprocess the CelebA dataset according to the method in [3]. Twelve attributes are selected to construct the attribute vector: hair color (black, blond, brown, gray), gender (male/female), age (young/old), expression (with/without smile), and hairstyle (with/without bangs). The quantitative and qualitative comparisons are shown in Table 8 and Fig. 9, and more visual results are presented in Fig. 10.

Table 8: Quantitative comparison of facial attribute transfer.

	FID	LPIPS
StarGAN	51.20	-
StarGAN*	48.16	0.001
DMIT	32.36	0.066



Figure 9: Qualitative comparison of facial attribute transfer. The styles of StarGAN* and DMIT are sampled from random noise.

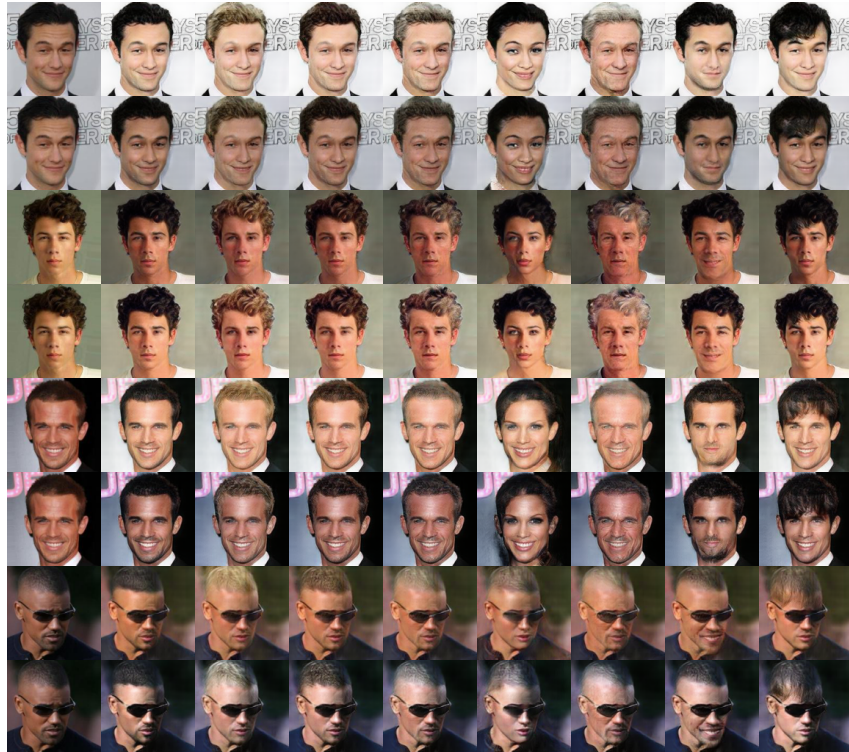


Figure 10: Facial attribute transfer results of DMIT on CelebA (Input, Black hair, Blond hair, Brown hair, Gray hair, Gender, Age, Smile, Bangs). Since "Old" and "Gray hair" are generally present at the same time in CelebA, we thus set the hair to gray to generate a realistic old face.

B.4 Sketch-to-Photo

We use the dataset provided by Isola *et al.* [16] to perform Sketch-to-Shoe and Shoe-to-Shoe translations. Our model in this task is trained with unpaired data, and the qualitative results are shown in Fig. 11



Figure 11: **Qualitative results of sketch-to-photo.** The first two rows show the inter-domain translation results of our model, and the last two rows shows the intra-domain translation results.